

Competition between Energy and Electron Transfer from CdSe QDs to Adsorbed Rhodamine B

Abdelaziz Boulesbaa,[†] Zhuangqun Huang,[†] David Wu, and Tianquan Lian*

Department of Chemistry, Emory University, Atlanta, Georgia 30322

Received: October 18, 2009; Revised Manuscript Received: November 24, 2009

Understanding the dynamics of exciton quenching in quantum dots (QDs) is essential to their potential applications, such as solar cells and biological imaging. In this work, the competition between electron and energy transfer from excited CdSe QDs to adsorbed rhodamine B (RhB) molecules was examined by time-resolved fluorescence decay, steady-state emission, and transient absorption measurements. The major pathway (84%) for exciton quenching in this system is through electron transfer to RhB, whereas $\sim 16\%$ of the excitons decay by energy transfer. In a sample with $\sim 2\text{--}3$ RhB per QD, exciton quenching occurs with an average time constant of 54 ps, and the charge-separated state has an average lifetime of 1 μs . The charge separation rate depends on the number of adsorbates attached to the QD, and the dependence can be well-described by a kinetics model that assumes a Poisson distribution of the number of adsorbates on the QDs.

Introduction

Understanding the dynamics of exciton quenching in quantum dots (QDs) is essential to their many potential applications, such as solar cells,^{1–3} light-emitting diodes,^{4–6} and biological imaging and detection.^{7–9} Quenching of QD excitons by Förster resonance energy transfer (FRET) to molecular acceptors, such as rhodamine, has been well-established, and various QD/dye molecule FRET pairs have been examined.^{9–13} Quenching of QD excitons by charge transfer to acceptors has also been reported.^{2,14–27} Interest in these processes has intensified in recent years because of reports of efficient multiexciton generation (MEG) in some QDs,^{28–39} which offers an exciting possibility to significantly enhance the efficiency of QD-based solar cells.^{40,41} In addition to understanding the mechanism, efficiency, and generality of MEG,^{42–49} it is also important to investigate how to utilize the multiexcitons before the ultrafast exciton–exciton annihilation process.^{50,51} Ultrafast charge and/or energy transfer to adsorbed molecular acceptors might provide potential approaches to separate multiexcitons before their annihilation.

Despite many reports of QD exciton quenching by either charge transfer or FRET, it is unclear how these processes compete with each other under conditions when both are energetically allowed. Many of the fluorescence dyes used as FRET acceptors in QD/dye complexes, such as rhodamine, can also serve as electron acceptors from QDs. The rate of FRET processes, resulting from the interaction between transition dipoles of the donor and acceptor, exhibits an r^{-6} dependence, where r is the donor–acceptor distance.⁵² On the other hand, the rate of electron transfer (ET) depends exponentially on the distance, decreasing much more rapidly with distance than the rate of FRET.^{53,54} At large distances, the ET rate is expected to become much smaller than the rate of FRET. At short distances, when the adsorbates are at the surface of the QD, both processes are expected to be fast. In our previous work, we demonstrated ultrafast electron transfer from CdS QDs to adsorbed rhodamine B (RhB) molecules.¹⁶ In a study of CdSe with attached rhodamine B derivative, efficient quenching of the CdSe

emission was reported and was attributed to energy transfer.¹⁰ Compared to that of CdS, the emission of CdSe is red-shifted and has a better overlap with RhB absorption, which likely leads to more efficient energy transfer to RhB. On the other hand, because of the similar positions of the conduction-band edges in CdS and CdSe, electron transfer from CdSe to RhB is also expected. CdSe/RhB therefore provides an interesting system in which to study the competition between the energy- and electron-transfer processes from QDs.

In this article, we present a study of the exciton quenching dynamics in CdSe/RhB. Exciton quenching was observed through the time-resolved fluorescence decay of CdSe. By direct probing of the products of the quenching process using transient absorption spectroscopy, electron transfer from CdSe to RhB was found to be the main quenching pathway. The efficiency of energy transfer was determined to be $\sim 16\%$ by steady-state emission. The exciton quenching rate was found to increase with the number of adsorbed RhB. Both fluorescence decay and transient absorption kinetics can be satisfactorily described by a model that assumes a Poisson distribution of the number of adsorbed molecules per QD.

Experimental Methods

Nanoparticle Synthesis. CdSe QDs capped with oleic acid (OA) were synthesized according to a previously published procedure.⁵⁵ In this case, 0.0640 g of CdO ($>99.99\%$, from Aldrich) was mixed with 9.00 mL of 1-octadecene (ODE, technical grade, 90%, from Aldrich) and 0.80 mL of OA (technical grade, 90%, from Aldrich). The mixture was heated to 320 °C under N_2 protection, and the resulting transparent solution was then cooled to 270 °C. A selenium stock solution containing 0.1021 g of Se ($>99.5\%$, 100 mesh, from Aldrich) dissolved in 2.65 mL of ODE and 0.35 mL of tributylphosphine (TBP, 97%, from Aldrich) was swiftly injected into the hot solution. The subsequent growth of CdSe nanoparticles was carried out at 250 °C. The reaction was stopped once the desired size of CdSe particles was reached.

CdSe/RhB complexes were prepared by addition of RhB to a CdSe QD solution in heptane, followed by sonication and

* To whom correspondence should be addressed. E-mail: tlian@emory.edu.

[†] These authors contributed equally to this work.

filtration to remove undissolved RhB molecules. The ratio of adsorbed RhB to QD was controlled by varying the amount of added RhB and was determined by ultraviolet/visible (UV/vis) absorption spectroscopy. Because RhB is insoluble in heptane, all dissolved dye molecules were believed to be bound to the CdSe QDs. A control sample without QDs showed no measurable RhB absorption. Furthermore, our previous fluorescence anisotropy measurements on a related system confirmed that RhB binds to CdS QDs.¹⁶

Ultrafast Visible and IR Transient Absorption Measurements. The ultrafast transient absorption (TA) spectrometer used in this study was based on a regeneratively amplified Ti:sapphire laser system (Coherent Legend, 800 nm, 150 fs, 2.5 mJ/pulse, and 1 kHz repetition rate). Pump pulses at 400 nm were generated by frequency doubling of the 800-nm pulse at a β -barium borate (BBO) crystal. Pump pulses at 532 nm were generated by sum-frequency generation using the signal output ($\sim 80 \mu\text{J}$) of an optical parametric amplifier (OPA, Clark-MXR, pumped with 1 mJ of the 800-nm pulse) and the 800-nm fundamental ($\sim 100 \mu\text{J}$). The energy of the pump pulse used for these measurements was controlled by a variable neutral-density (ND) filter wheel. The pump beam size at the sample was adjusted to be $\sim 400 \mu\text{m}$.

A white-light-continuum (WLC, from 400 to 750 nm) probe was generated by attenuating and focusing $\sim 10 \mu\text{J}$ of the 800-nm pulse into a rotating 2-mm-thick CaF_2 window. The WLC was collimated and then focused onto the sample using protected Al off-axis parabolic reflectors to give a beam size of $\sim 75 \mu\text{m}$. After the sample, the probe was collimated and focused into a fiber-coupled spectrometer [Ocean Optics HR2000Plus, 2048-pixel charge-coupled device (CCD), 0.25 nm/pixel readout] and detected at a frequency of 10 Hz. The pump pulses were chopped by a synchronized chopper (New Focus 3500) to the same frequency. Zero time delay and the instrument response function were obtained with the instantaneous exciton bleach at 480 nm of CdSe in heptane solution. During data collection, samples were constantly translated at a speed of 10 mm/min to avoid long-term photodegradation. For transient absorption measurements, samples were sealed in Harrick IR cells with a $400 \mu\text{m}$ -thick spacer sandwiched between two sapphire windows.

The tunable infrared probe was generated using an IR OPA (Coherent OPerA). The IR OPA was pumped at 800 nm (1 mJ/pulse) to produce signal and idler outputs at 1337 and 1992 nm, respectively. The signal and idler were collinearly mixed in a AgGaS_2 crystal to produce, by difference-frequency generation, tunable mid-IR probe pulses with a full width at half-maximum (fwhm) of $\sim 120 \text{ cm}^{-1}$ and a pulse energy of $\sim 5 \mu\text{J}$ at $\sim 4070 \text{ nm}$. The IR probe pulses were attenuated to $\sim 10 \text{ nJ}$ with a beam splitter and ND filters and chirp-corrected with Ge windows before the sample. The IR probe was focused onto the sample using protected Au parabolic reflectors to give a beam size of $\sim 180 \mu\text{m}$. After the sample, the probe (centered at 2450 cm^{-1}) was dispersed in a spectrometer with a resolution of 15 nm (5.4 cm^{-1} at 2450 cm^{-1}) and detected with a 32-element mercury cadmium telluride (MCT) array detector. Every other pump pulse was blocked by a synchronized chopper at a frequency of 500 Hz, and the absorbance change was calculated from the intensities of sequential probe pulses with and without the pump.

Nanosecond Transient Absorption Measurements. Nanosecond transient absorption was performed with an EOS spectrometer (Ultrafast Systems LLC). The pump pulses at 400 nm were from the femtosecond amplified laser system described above. The probe pulse (a 0.5-ns white-light source operating

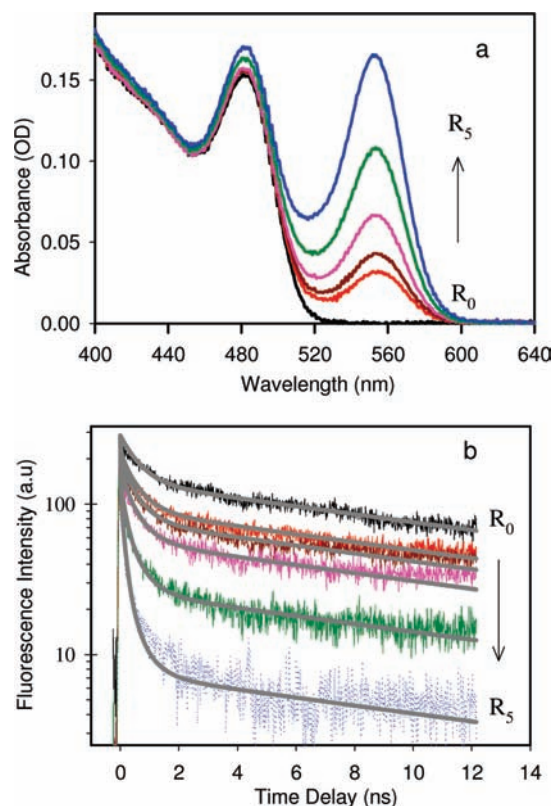


Figure 1. (a) UV/vis absorption spectra and (b) QD fluorescence decays of CdSe QD (R_0) and QD/RhB (R_1 – R_5). Samples R_0 – R_5 contained the same concentration of QDs but increasing amount of RhB. Solid lines in b are fits according to the model described in the main text.

at 20 kHz) was synchronized with the femtosecond amplifier, and the delay time was controlled by a digital delay generator. The probe light was detected in a fiber-optics-coupled multi-channel spectrometer with a complementary metal–oxide–semiconductor (CMOS) sensor. The absorbance change was calculated from the intensities of sequential probe pulses with and without the pump.

Static and Time-Resolved Fluorescence Measurements. Steady-state emission spectra of the samples were measured using a SPEX FluoroLog-3 self-contained and fully automated spectrofluorometer. Time-resolved fluorescence measurements were performed in the time-correlated single-photon-counting (TCSPC) mode under a right-angle sample geometry. A femtosecond laser pulse (100 fs) with a repetition rate of 80 MHz was generated from a mode-locked Ti:sapphire laser (Tsunami oscillator pumped by 10 W Millennium Pro, Spectra-Physics). The output centered at 400 nm was doubled through a BBO crystal to generate 400-nm excitation pulses. The emission was detected by a microchannel-plate photomultiplier tube (Hamamatsu R3809U-51), whose output was amplified and analyzed by a TCSPC board (Becker & Hickel SPC 600).

Results

Exciton Quenching Probed by Time-Resolved Fluorescence Decay. Figure 1a shows UV/vis absorption spectra of the CdSe/RhB samples used for the transient absorption and fluorescence decay measurements. Sample R_0 is CdSe only, and from sample R_1 to sample R_5 , the QD concentration remains the same as in R_0 but the amount of adsorbed RhB increases. The lowest-energy allowed exciton transition [$1S_{3/2}(h)$ – $1S_{1/2}(e)$], denoting a hole in the $1S_{3/2}$ level of the valence band and an

TABLE 1: Fitting Parameters for the Fluorescence Decay (FD) and Transient Absorption (TA) Kinetics of CdSe and CdSe/RhB^a

	free QD decay kinetics			ET kinetics	
	1/ <i>k</i> ₀₁ , ns (<i>B</i> ₁ , %)	1/ <i>k</i> ₀₂ , ns (<i>B</i> ₂ , %)	1/ <i>k</i> ₀₃ , ns (<i>B</i> ₃ , %)	1/ <i>k</i> ₁₁ , ps (<i>A</i> ₁ , %)	1/ <i>k</i> ₁₂ , ps (<i>A</i> ₂ , %)
FD	36 (29)	5.8 (27)	0.5 (43)	7.3 (43)	170 (57)
TA	27 (84)	0.002 (16)			

sample	RhB/QD ratio					
	R ₀	R ₁	R ₂	R ₃	R ₄	R ₅
<i>m</i> (FD)	0	0.4	0.6	0.9	1.6	2.6
<i>m</i> (TA)	0	0.4	0.6	0.9	1.5	2.2

^a *A*_{*j*}, *k*_{*1j*}, *B*_{*i*}, *k*_{*0i*} (*i, j* = 1, 2, 3) and *m* are fitting parameters using eq 7.

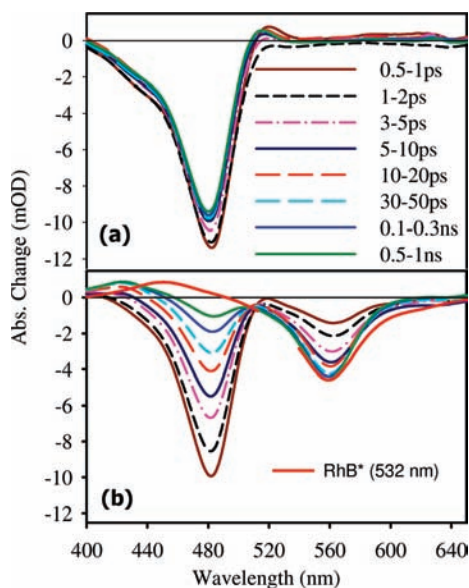


Figure 2. Transient absorption spectra recorded after 400-nm excitation at low pump density ($13 \mu\text{J}/\text{cm}^2$) for (a) CdSe (R_0) and (b) CdSe/RhB (R_5). Also shown in b is the spectrum of excited RhB (RhB^*) measured in sample R_5 at 1 ns after 532-nm excitation of RhB (solid red line). Each transient spectrum is an average of spectra in the indicated range time delays.

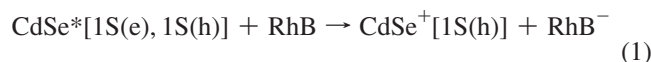
electron in the $1S_{1/2}$ level of the conduction band] of these QDs peaks at 480 nm, corresponding to an estimated radius of 1.95 nm.^{56,57} The time-resolved fluorescence decays of samples R_0 – R_5 are compared in Figure 1b. They were obtained by preferentially exciting the QD at 400 nm and collecting the QD band-edge emission around 483–493 nm. A control experiment with RhB in ethanol confirmed that RhB emission makes a negligible contribution to the obtained results (data not shown). In the absence of RhB, the QD exciton decay can be fitted by a three-exponential decay function. The fitting parameters are listed in Table 1. The amplitude-weighted average time constant was calculated to be 12.2 ns. With adsorbed RhB, fast decay components appear, and the amplitudes and decay rates of these components increase with the number of adsorbed RhB molecules, indicating the quenching of CdSe emission by the RhB molecules.

Transient Absorption Study of Exciton Quenching Pathways. Exciton quenching can be caused by electron, hole, or energy transfer from excited CdSe QDs to RhB molecules. These processes produce different products that can be distinguished by transient absorption spectroscopy. Shown in Figure

2 is a comparison of the transient absorption spectra of samples R_0 and R_5 recorded after 400-nm excitation (with a power density of $\sim 13 \mu\text{J}/\text{cm}^2$). The transient absorption spectra of sample R_0 (CdSe only) show two features: a bleach of the $1S_{1/2}(e) - 1S_{3/2}(h)$ exciton transition at 480 nm and a positive absorption at ~ 520 nm. The two features have been attributed to the presence of $1S$ electrons in QDs, which leads to the filling of the $1S_{1/2}(e)$ level, reducing the QD exciton absorption (hence the formation of the bleach), and a red-shift of the exciton absorption peak due to Coulomb interaction.^{50,58–62}

The exciton bleach recovers by $\sim 15\%$ in the first 10 ps and remains nearly constant from 10 ps to 1 ns. The fast initial recovery might indicate multiple excitations and the fast exciton–exciton annihilation in 15% of quantum dots. Most of the excited electrons remain in the $1S$ level for over 1 ns in free QDs. Within the same time window, the fluorescence intensity decays by 40% (Figure 1b). This suggests that $\sim 40\%$ of the holes are trapped within ~ 1 ns in free QDs.

In the presence of RhB, as shown in Figure 2b, the transient absorption spectra of CdSe/RhB showed a fast recovery of the exciton bleach and a corresponding formation of the RhB ground-state bleach at 550 nm and a new positive absorption band centered at ~ 425 nm. This new absorption band can be assigned to reduced RhB (RhB^-),^{16,63} indicating that excitons dissociate by electron transfer from the QD to RhB



To further support this assignment, we also generated a difference spectrum of the RhB excited state by directly exciting RhB at 532 nm in sample R_5 . As shown in Figure 2b, in addition to the bleach of RhB ground state, this excited-state absorption spectrum exhibits an absorption peak at 450 nm and stimulated emission features at 560–650 nm. These latter features are distinctly different from those observed with 400-nm excitation of CdSe, suggesting that energy transfer is not the main exciton quenching pathway.

The kinetics of exciton quenching can be probed by following the exciton bleach recovery (480 nm) and the formation of the RhB ground-state bleach (550 nm). Furthermore, the kinetics of the $1S$ electrons can also be monitored by the $1S(e) \rightarrow 1P(e)$ intraband transition in the mid-IR region.^{58,64} For this measurement, electrons in the CdSe $1S$ level were probed at 2450 cm^{-1} following 400-nm excitation. As shown in Figure 3a, in sample R_0 , the optical excitation of the QDs leads to the instantaneous formation of an electron intraband absorption that follows the same kinetics as the exciton bleach signal (probed at 480 nm).

In the presence of RhB (in sample R_5), the intraband absorption signal at 2450 cm^{-1} decays rapidly, and its decay kinetics agrees with the exciton bleach recovery at 480 nm. The decays of these conduction-band electron signatures agree well with the RhB bleach formation at 550 nm within the first 50 ps. At longer delay times, the amplitude of the RhB bleach decreases, and its kinetics deviates from the decay of the conduction-band electron signals. The origin of this difference is not clear. It might indicate the onset of charge recombination, which leads to the decay of the RhB bleach. It might also indicate the occurrence of a small extent of energy-transfer processes, producing excited RhB that decays on the time scale of a few nanoseconds. The comparison described above suggests that exciton bleach recovery kinetics can be used to follow the kinetics of $1S$ electrons, as was shown previously in other systems.^{17,26}

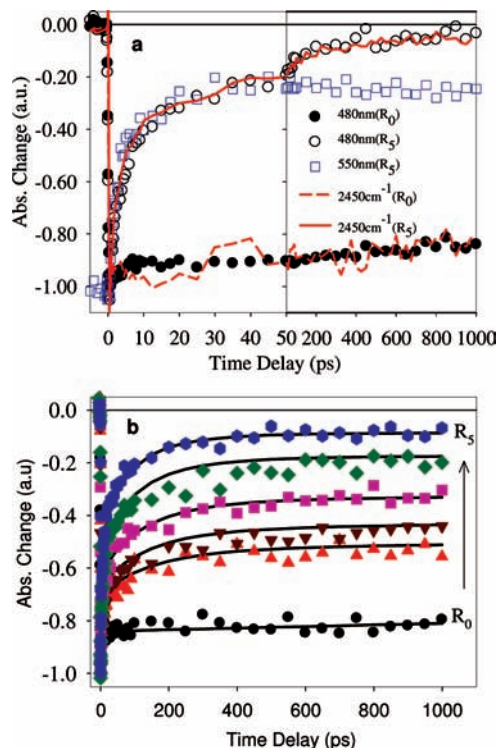


Figure 3. (a) Transient absorption kinetics of samples R_0 and R_5 following 400-nm excitation at low pump density ($13 \mu\text{J}/\text{cm}^2$): QD exciton bleach recovery at 480 nm in R_0 (filled circles) and R_5 (open circles), RhB bleach formation at 550 nm in R_5 (open squares), and QD intraband absorption at 2450 cm^{-1} in R_0 (dashed line) and R_5 (solid line). IR absorption kinetic traces are inverted for better comparison with bleach recovery. The RhB bleach has also been inverted and displaced vertically to facilitate the comparison of its formation with the recovery of the exciton bleach. (b) Comparison of QD exciton bleach recovery kinetics in sample R_0 – R_5 . Solid lines are fits according to the model described in the main text.

In addition to samples R_0 and R_5 , the transient absorption spectra for samples R_1 – R_4 were measured and analyzed in the same way. Shown in Figure 3b is a comparison of the QD exciton bleach recovery kinetics in samples R_0 – R_5 . The rate of bleach recovery increases with the number of adsorbed RhB molecules per CdSe QD, consistent with the emission quenching results shown in Figure 1b. A model that can account for the observed adsorbate-dependent quenching kinetics is described later in the Discussion section.

Transient Absorption Study of the Charge Recombination Process. The charge-separated state (with an electron in RhB and a hole in CdSe) eventually recombines to regenerate CdSe and RhB according to the equation



To investigate this process, we also measured the transient absorption spectra of CdSe/RhB (sample R_6 ; absorption spectrum shown in Figure S1, Supporting Information) from 1 ns to $4 \mu\text{s}$ using a nanosecond transient absorption setup. As shown in Figure 4a, the CdSe exciton bleach decays completely after 20 ns, whereas the RhB^- absorption (420 nm) and the RhB ground-state bleach (550 nm) decay on the microsecond time scale, suggesting a long-lived charge-separated state. The observed bleach of RhB on the >20 -ns time scale cannot be attributed to excited RhB^* , which has a lifetime of ~ 3 ns. This

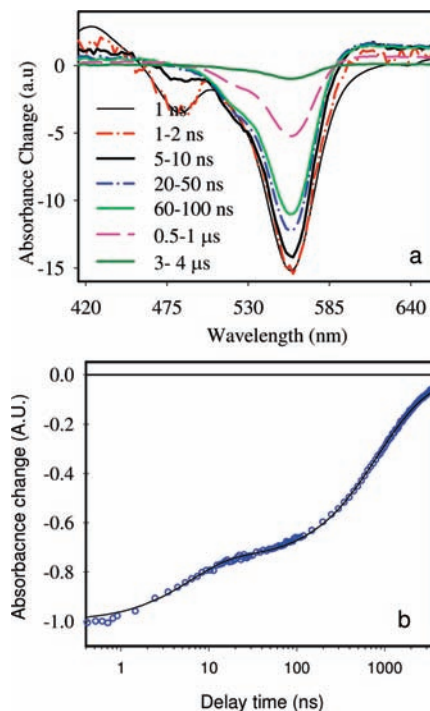


Figure 4. (a) Transient absorption spectra at the indicated time delays (1 ns to $4 \mu\text{s}$) and of CdSe/RhB (sample R_6) measured after 400-nm excitation. Also shown for comparison is a transient spectrum at 1 ns (thin black line) recorded with a femtosecond transient spectrometer (see Figure 2b). Each transient spectrum is an average of spectra in the indicated range of time delays. (b) Kinetics trace of RhB bleach recovery at 550 nm (open circles) and fit to a three-exponential decay function (solid line).

result further confirms that the main exciton quenching pathway is by electron transfer to RhB.

The charge recombination kinetics can be monitored by the RhB ground-state bleach recovery, as shown in Figure 4b. The recovery of the RhB bleach can be fitted by a three-exponential decay function with amplitudes and time constants of 25%, 6 ns; 49%, 680 ns; and 28%, 2406 ns. From these parameters, an amplitude-weighted average time constant of $1 \mu\text{s}$ for the charge recombination process was obtained. It should be noted that the charge recombination starts on the ~ 100 -ps time scale, as shown in Figure 3a, and is not completed at $4 \mu\text{s}$. The origin for this highly non-single-exponential electron-transfer process is unclear.

Quantification of Energy-Transfer Efficiency by Steady-State Emission. Although the transient absorption data clearly show that electron transfer is the main exciton quenching pathway, they cannot exclude the possibility of a small contribution from energy transfer because of the limited signal-to-noise ratio of the data. The contribution of energy transfer can be more accurately determined by measuring the steady-state emission of RhB. Therefore, we compared the RhB emissions from samples of CdSe and CdSe/RhB (sample R_6) with the same QD absorbance (see Figure S1, Supporting Information). As shown in Figure 5, the emission spectra (resulting from 400-nm excitation) demonstrate that, in the presence of RhB, the CdSe emission is almost completely quenched, and there is noticeable RhB emission (I_{QRhB}). RhB emission can result from energy transfer from excited QDs as well as direct excitation of RhB, because RhB has a small absorbance at 400 nm. The contribution of the latter can be determined by comparison with a sample of RhB in ethanol that has the same RhB absorbance as in CdSe/RhB. As shown

in Figure 5, the RhB emission in RhB/ethanol solution is weaker than that in CdSe/RhB. This suggests that the observed emission in CdSe/RhB cannot be explained by the direct excitation of RhB alone and that there must be energy transfer from excited CdSe {CdSe*[1S(e),1S(h)]} to RhB



To further confirm the energy-transfer process, we also measured the rise time of RhB emission by the TCSPC technique. The rise time should be instrument-response-limited if it is due to direct excitation of RhB. On the other hand, if it results from energy transfer from the QDs, the rise time should be the same as the decay time of QD emission. As shown in Figure S4 (Supporting Information), the growth of RhB emission is similar to the decay of CdSe emission, suggesting that energy transfer from CdSe to RhB is responsible for the observed RhB emission.

To quantify the energy-transfer efficiency, the fluorescence quantum yields for CdSe in heptane, RhB in ethanol, and RhB on CdSe were also determined. As described in the Supporting Information (Figure S2), using coumarin 343 ($\Phi_{\text{C343}} \approx 0.63^{65}$) and RhB 101 ($\Phi_{\text{RhB101}} \approx 1.00^{66}$) as standard samples (for 400- and 550-nm excitation, respectively), the quantum yields of CdSe (Φ_{QD} , 400-nm excitation), RhB in ethanol (Φ_{RhB} , 550 nm excitation), and RhB on CdSe in heptane (Φ_{QRhB} , 550-nm excitation) were found to be 0.10, 0.68, and 0.38, respectively. The value for RhB in ethanol is similar to reported values,⁶⁶ confirming the accuracy of our measurements. The reason for the lower quantum yield for RhB adsorbed on CdSe is unclear.

The amount of RhB emission in RhB/CdSe due to direct excitation at 400 nm (I_{dRhB}) can be estimated from the measured RhB emission intensity in the absence of QDs. The presence of QDs reduces the amount of photons absorbed by RhB. By accounting for this internal filter effect and the difference between the fluorescence quantum yields of free RhB in solution and adsorbed RhB on CdSe, I_{dRhB} was estimated to be 15% of the total emission of RhB. The energy-transfer efficiency (η) was then calculated as

$$\eta = \frac{(I_{\text{QRhB}} - I_{\text{dRhB}})/\Phi_{\text{QRhB}}}{I_{\text{QD}}/\Phi_{\text{QD}}} \quad (4)$$

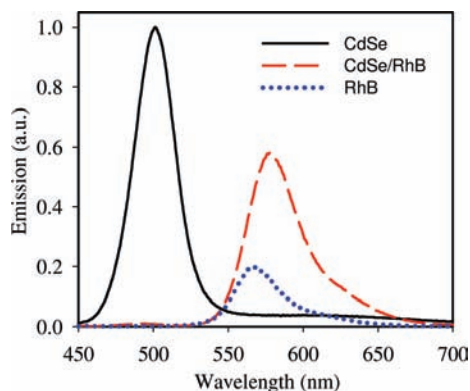


Figure 5. Static emission spectra of samples containing CdSe (black solid line), CdSe/RhB (red dashed line), and RhB (blue dash-dotted line) after 400-nm excitation. The absorption spectra of these samples are shown in Figure S1 (Supporting Information).

where I_{QD} is the exciton emission intensity of CdSe (without RhB). All emission intensities were obtained by integrating the emission spectra. The η value for this sample was estimated to be $\sim 16\%$.

Discussion

Adsorbate/QD Ratio Dependence of Exciton Quenching Kinetics. It is interesting to note that, in Figure 1b, the fluorescence decays between 4 and 12 ns have the same rate in all samples, identical to that of free QDs. The amplitudes decrease from R_0 to R_5 , suggesting the presence of decreasing amounts of free QDs in these samples. The presence of free QDs in samples with average numbers of RhB per QD above 1 indicates that there is a distribution of the number of adsorbates on the QDs. Therefore, a quantitative interpretation of the measured kinetics would require a model that accounts for this distribution. If the adsorption process is random (i.e., the probability of adsorbing a molecule is independent of the number of molecules already adsorbed), then the number of adsorbates on the QDs should obey a Poisson distribution^{18,67}

$$f_n = \sum_n \frac{m^n}{n!} e^{-m} \quad (5)$$

where f_n is the probability of QDs with n adsorbed molecules and m is the average number of adsorbates per QD. We assume that the exciton decay kinetics in QD/ n RhB (1: n) complexes is described by a multiexponential function with amplitude and rate constant of A_j and k_{nj} , respectively. It is further assumed that these rate constants are linearly proportional to the number of adsorbates per QD

$$k_{nj} = nk_{1j} \quad (6)$$

where k_{nj} and k_{1j} are the j th components of the exciton quenching constants for the 1: n and 1:1 CdSe/RhB systems, respectively. It can be shown that, for a sample with an average of m adsorbates per QD, the concentration of excited QDs at delay time t , $[N_i^*]$, is^{18,68,69}

$$[N_i^*] = [N_0^*] \left[\sum_j A_j \exp(-m + me^{-k_{1j}t}) \right] \left(\sum_i B_i e^{-k_{0i}t} \right) \quad (7)$$

where $[N_0^*]$ is the initial concentration of excited QDs and B_i and k_{0i} are the amplitude and decay time constant, respectively, of the i th component of the multiexponential decay kinetics of excited free QDs (without RhB).

The fluorescence intensity should depend linearly on the concentration of excited QDs. All transient absorption measurements were carried out under low excitation density, in which the average number of excitons per QD was much less than 1 and the contributions from QDs with multiple excitons were negligible. Under these conditions, the amplitude of QD exciton bleach measured in transient absorption should also be linearly dependent on the concentration of excited QDs. Equation 7 can be used to fit the kinetics of both transient absorption (Figure 1c) and fluorescence decay (Figure 1b).

The kinetics of free QDs (R_0 , $m = 0$) was first fitted to obtain the values of B_i and k_{0i} . These parameters are different for the fluorescence decay and transient absorption kinetics and are included in Table 1. The decay kinetics of R_1 – R_5 were then fit

using the same values of A_j and k_{1j} and varying values of m . The best fits to these decay kinetics are shown in Figures 1b and 3b, and the fitting parameters, A_j , k_{1j} , and m , are also listed in Table 1. The model appears to give a reasonable description of the measured fluorescence and transient absorption kinetics. Because the same samples were measured by both transient absorption and fluorescence decay, we used same ET parameters, A_j and k_{1j} , in these fits. Furthermore, for a given sample, m values obtained from the fits to the fluorescence and transient data should be the same. Indeed, these values agree well with each other, except for the sample with the highest ratio of adsorbate molecules.

Energy- and Electron-Transfer Rates. Assuming that the energy- and electron-transfer rates are both linearly dependent on the number of adsorbate molecules, the energy-transfer efficiency should be independent of the adsorbate/QD ratio. According to the model described in the preceding section, the amplitude-weighted average time constant for exciton quenching in the 1:1 CdSe/RhB complex is ~ 100 ps. With an energy-transfer efficiency of 16%, the average electron- and energy-transfer times can be estimated as 120 and 620 ps, respectively. In QDs with adsorbed RhB molecules (one or more), the quenching of excitons by either energy (16%) or electron transfer (84%) is nearly 100%. For sample R₅, with an estimated 2–3 adsorbed RhB molecules per QD, the average time constant of exciton quenching is 54 ps, and the average electron- and energy-transfer times are ~ 64 and 340 ps, respectively. The percentage of free QDs in the solution is $\sim 8\%$ according to the Poisson distribution, which accounts for the small amount of long-lived exciton signals in the sample (fluorescence intensity in Figure 1b and exciton bleach in Figure 3b).

Previous studies have shown that energy transfer between quantum dots and molecular acceptors can be described well by FRET.¹¹ From the measured absorption spectrum of RhB and the emission spectrum of CdSe, the calculated Förster radius of a 1:1 CdSe/RhB pair is 3.53 nm. The details of the calculation can be found in the Supporting Information. Assuming a distance from RhB to the center of the QD in the range between 1.9 nm (the radius of a QD) and 2.3 nm (the radius of a QD plus one-half the size of the RhB) and using an average lifetime of free QDs of 12.2 ns, the FRET rate (k_{ent}) can be estimated as between 0.9×10^9 and $3.1 \times 10^9 \text{ s}^{-1}$ (or time constants between 1.1 ns and 320 ps) in the 1:1 QD/RhB complexes. This estimated FRET time is consistent with the value (~ 620 ps) derived from the measured exciton quenching rate described above.

Under our experimental conditions, in which the average number of excitons per quantum dot is less than 1, the charge-separated state consists of one electron in the adsorbate and a hole in the QD, regardless of the number of adsorbates. Therefore, the recombination process should be independent of the number of adsorbates. According to the transient kinetics shown in Figure 4, the average charge recombination time is 1 μs , which is about 8300 times slower than charge separation in a 1:1 QD/RhB complex. The reason for the large difference between the charge separation and recombination rates is unclear. According to Marcus' theory of nonadiabatic electron transfer, the rate of electron transfer depends on the driving force (the free energy change of the reaction), the reorganization energy, and the electronic coupling strength.⁷⁰ The excited-state oxidation and reduction potentials of CdSe (1S exciton peak at 480 nm) can be estimated as -1.37 and 1.10 V (vs SCE), respectively, following the model of Brus.^{56,57} From the reported reduction potential for RhB of -0.8 V (SCE),⁷¹ the driving forces of charge separation (eq 1) and recombination (eq 2) are

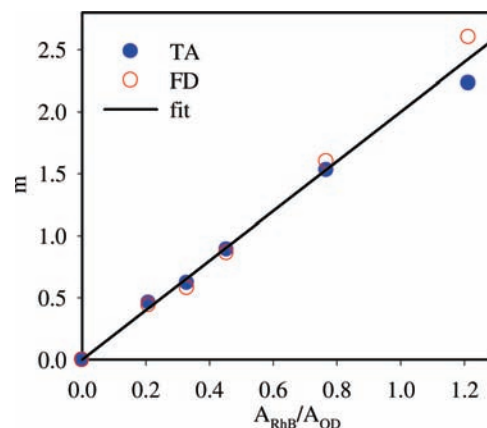


Figure 6. Average number of RhB molecules per QD (m) as a function of the ratio of the absorbance of RhB (at 550 nm) vs QD (at 480 nm). m values were obtained by fitting the transient absorption (filled circles) and fluorescence decay (open circles) data as described in the text. The solid line represents a linear fit to these data with a slope of 2.0.

-0.56 and -1.9 V, respectively. The total reorganization energy includes the vibrational reorganization energy (due to changes in bond lengths and geometry) and solvent reorganization. The vibrational reorganization energy of QDs has not been reported. However, it can be expected to be small for the electron-transfer process because of the delocalized nature of the 1S electron. The vibrational reorganization energy for many organic chromophores has been estimated to be around 0.05 eV,^{72,73} although a value as high as 0.43 eV was determined in a hexamethylbenzene/tetracyanoethylene charge-transfer complex.⁷⁴ In non-polar solvents similar to heptane, the solvent reorganization energy is often small. For example, in benzene, the solvent reorganization is 0.008 V according to the dielectric continuum model and 0.178 V according to a molecular solvation model.⁷⁵ Thus, the total reorganization energy can be estimated to be around 0.2–0.6 V. Because of the uncertainties in the total reorganization energy and in the driving force, it is unclear whether the forward reaction is in the Marcus normal regime. The charge recombination process, with a driving force of -1.9 eV, likely falls in the inverted regime, which might be partially responsible for the much lower charge recombination rate.⁵³ Additionally, the electronic coupling strengths for these ET processes might be quite different. In the charge separation process, the coupling is determined by the overlap of 1S_{1/2} electron wave function with the accepting orbital of the RhB. The recombination process involves the wave function of valence-band or trapped holes. As discussed earlier, 40% of valence holes can be trapped within 1 ns. It is likely that the localized wave function of the trapped holes reduces their overlap with the adsorbate and slows the recombination process.

Extinction Coefficients of QD. The average number of RhB molecules per QD, m , can also be calculated from the absorbance (A) and extinction coefficient (ϵ) values of QDs and RhB

$$m = \frac{A_{\text{RhB}}/A_{\text{QD}}}{\epsilon_{\text{RhB}}/\epsilon_{\text{QD}}} = \frac{\epsilon_{\text{QD}} A_{\text{RhB}}}{\epsilon_{\text{RhB}} A_{\text{QD}}} \quad (8)$$

Plotting the m values obtained from the fit described above against the ratio of the absorbances of RhB (at its peak, 550 nm) and QD (at the first exciton peak, 480 nm) should yield a straight line with a slope that is determined by the ratio of their extinction coefficients. As shown in Figure 6, such a plot can indeed be fit by a straight line with a slope of ~ 2 . Using the

known extinction coefficient of RhB at 550 nm ($\epsilon_{\text{RhB}} = 106000 \text{ M}^{-1}\text{cm}^{-1}$),⁷⁶ we obtained a value for ϵ_{QD} of $\sim 212000 \text{ M}^{-1}\text{cm}^{-1}$. The calculated extinction coefficient of CdSe QDs according to a published empirical formula is $\sim 46000 \text{ M}^{-1}\text{cm}^{-1}$, which is about 4.6 times smaller than the value obtained here.⁷⁷ Furthermore, the QD radius estimated from this empirical formula also predicts a FRET rate that is much higher than the measured value. Although the accuracy of the reported QD extinction coefficient is quite poor at this small size⁷⁷ and has been questioned,¹⁰ it is unclear whether a lack of accuracy can account for the large discrepancy observed here. Another possibility is that the assumption of a Poisson distribution might be invalid. This model, which assumes a random adsorption process, can be valid only when the interaction between the adsorbates is negligible compared to their interaction with the QDs and when the number of adsorption sites is much larger than the number of adsorbed molecules. The validity of the model will be further tested in future studies. One possible approach might be to directly measure the distribution of the number of adsorbates on the QDs by single-molecule spectroscopy.¹⁵

Conclusions

The pathways for the quenching of QD excitons in CdSe/RhB complexes were examined by time-resolved fluorescence decay, steady-state emission, and transient absorption spectroscopy. It was shown that exciton dissociation by electron transfer to adsorbed RhB is the dominating quenching pathway, whereas energy transfer accounts for only 16%. In a sample with ~ 2 – 3 adsorbates per QD, exciton quenching was found to occur with an average time constant of 54 ps. The charge-separated state was found to be long-lived, with an average lifetime of 1 μs . The exciton quenching rate was found to increase with the number of adsorbates attached to the QD. The dependence of the quenching kinetics on the number of adsorbates can be well-described by a kinetics model that assumes a Poisson distribution of adsorbate molecules on the QDs.

Acknowledgment. This work was supported by Basic Energy Science of the U.S. Department of Energy (DE-FG02-07ER-15906) and in part by the Petroleum Research Fund (PRF #49286-ND6). T.L. thanks Dr. M. Tachiya for helpful discussions on the kinetics model used in this work.

Supporting Information Available: Spectra, kinetics, and analysis of energy transfer. This information is available free of charge via the Internet at <http://pubs.acs.org>.

References and Notes

- (1) Huynh, W. U.; Dittmer, J. J.; Alivisatos, A. P. *Science* **2002**, *295*, 2425.
- (2) Robel, I.; Subramanian, V.; Kuno, M.; Kamat, P. V. *J. Am. Chem. Soc.* **2006**, *128*, 2385.
- (3) Tachibana, Y.; Akiyama, H. Y.; Ohtsuka, Y.; Torimoto, T.; Kuwabata, S. *Chem. Lett.* **2007**, *36*, 88.
- (4) Achermann, M.; Petruska, M. A.; Koleske, D. D.; Crawford, M. H.; Klimov, V. I. *Nano Lett.* **2006**, *6*, 1396.
- (5) Steckel, J. S.; Snee, P.; Coe-Sullivan, S.; Zimmer, J. P.; Halpert, J. E.; Anikeeva, P.; Kim, L.-A.; Bulovic, V.; Bawendi, M. G. *Angew. Chem., Int. Ed.* **2006**, *45*, 5796.
- (6) Colvin, V. L.; Schlamp, M. C.; Alivisatos, A. P. *Nature* **1994**, *370*, 354.
- (7) Bruchez, M.; Moronne, M.; Gin, P.; Weiss, S.; Alivisatos, A. P. *Science* **1998**, *281*, 2013.
- (8) Chan, W. C. W.; Nie, S. *Science* **1998**, *281*, 2016.
- (9) Medintz, I. L.; Clapp, A. R.; Brunel, F. M.; Tiefenbrunn, T.; Uydea, H. T.; Chang, E. L.; Deschamps, J. R.; Dawson, P. E.; Mattoussi, H. *Nat. Mater.* **2006**, *5*, 581.

- (10) Funston, A. M.; Jasieniak, J. J.; Mulvaney, P. *Adv. Mater.* **2008**, *20*, 4274.
- (11) Curutchet, C.; Franceschetti, A.; Zunger, A.; Scholes, G. D. *J. Phys. Chem. C* **2008**, *112*, 13336.
- (12) Medintz, I. L.; Mattoussi, H. *Phys. Chem. Chem. Phys.* **2009**, *11*, 17.
- (13) Dayal, S.; Burda, C. *J. Am. Chem. Soc.* **2007**, *129*, 7977.
- (14) Kamat, P. J. *J. Phys. Chem. C* **2008**, *112*, 18737.
- (15) Issac, A.; Jin, S.; Lian, T. *J. Am. Chem. Soc.* **2008**, *130*, 11280.
- (16) Boulesbaa, A.; Issac, A.; Stockwell, D.; Huang, Z.; Huang, J.; Guo, J.; Lian, T. *J. Am. Chem. Soc.* **2007**, *129*, 15132.
- (17) Huang, J.; Stockwell, D.; Huang, Z.; Mohler, D. L.; Lian, T. *J. Am. Chem. Soc.* **2008**, *130*, 5632.
- (18) Huang, J.; Huang, Z.; Jin, S.; Lian, T. *J. Phys. Chem. C* **2008**, *112*, 19734.
- (19) Rossetti, R.; Beck, S. M.; Brus, L. E. *J. Am. Chem. Soc.* **1984**, *106*, 980.
- (20) Rossetti, R.; Brus, L. E. *J. Phys. Chem.* **1986**, *90*, 558.
- (21) Ramsden, J. J.; Gratzel, M. *Chem. Phys. Lett.* **1986**, *132*, 269.
- (22) Henglein, A. *Pure Appl. Chem.* **1984**, *56*, 1215.
- (23) Logunov, S.; Green, T.; Marguet, S.; El-Sayed, M. A. *J. Phys. Chem. A* **1998**, *102*, 5652.
- (24) Burda, C.; Green, T. C.; Link, S.; El-Sayed, M. A. *J. Phys. Chem. B* **1999**, *103*, 1783.
- (25) Blackburn, J. L.; Ellingson, R. J.; Micic, O. I.; Nozik, A. J. *J. Phys. Chem. B* **2003**, *107*, 102.
- (26) Robel, I.; Kuno, M.; Kamat, P. V. *J. Am. Chem. Soc.* **2007**, *129*, 4136.
- (27) Spanhel, I.; Weller, H.; Henglein, A. *J. Am. Chem. Soc.* **1987**, *109*, 6632.
- (28) Pietryga, J. M.; Schaller, R. D.; Werder, D.; Stewart, M. H.; Klimov, V. I.; Hollingsworth, J. A. *J. Am. Chem. Soc.* **2004**, *126*, 11752.
- (29) Ellingson, R. J.; Beard, M. C.; Johnson, J. C.; Yu, P.; Micic, O. I.; Nozik, A. J.; Shabaev, A.; Efros, A. L. *Nano Lett.* **2005**, *5*, 865.
- (30) Luther, J. M.; Beard, M. C.; Song, Q.; Law, M.; Ellingson, R. J.; Nozik, A. J. *Nano Lett.* **2007**, *7*, 1779.
- (31) Schaller, R. D.; Sykora, M.; Jeong, S.; Klimov, V. I. *J. Phys. Chem. B* **2006**, *110*, 25332.
- (32) Trinh, M. T.; Houtepen, A. J.; Schins, J. M.; Hanrath, T.; Piris, J.; Knulst, W.; Goossens, A. P. L. M.; Siebbeles, L. D. A. *Nano Lett.* **2008**, *8*, 1713.
- (33) Murphy, J. E.; Beard, M. C.; Norman, A. G.; Ahrenkiel, S. P.; Johnson, J. C.; Yu, P.; Micic, O. I.; Ellingson, R. J.; Nozik, A. J. *J. Am. Chem. Soc.* **2006**, *128*, 3241.
- (34) Beard, M. C.; Knutsen, K. P.; Yu, P.; Luther, J. M.; Song, Q.; Metzger, W. K.; Ellingson, R. J.; Nozik, A. J. *Nano Lett.* **2007**, *7*, 2506.
- (35) Sykora, M.; Mangolini, L.; Schaller, R. D.; Kortshagen, U.; Jurbergs, D.; Klimov, V. I. *Phys. Rev. Lett.* **2008**, *100*, 067401/1.
- (36) Schaller, R. D.; Petruska, M. A.; Klimov, V. I. *Appl. Phys. Lett.* **2005**, *87*, 253102/1.
- (37) Schaller, R. D.; Pietryga, J. M.; Klimov, V. I. *Nano Lett.* **2007**, *7*, 3469.
- (38) Pijpers, J. J. H.; Hendry, E.; Milder, M. T. W.; Fanciulli, R.; Savolainen, J.; Herek, J. L.; Vanmaekelbergh, D.; Ruhman, S.; Mocatta, D.; Oron, D.; Aharoni, A.; Banin, U.; Bonn, M. *J. Phys. Chem. C* **2007**, *111*, 4146.
- (39) Sukhovatkin, V.; Hinds, S.; Brzozowski, L.; Sargent, E. H. *Science* **2009**, *324*, 1542.
- (40) Nozik, A. J. *Physica E* **2002**, *14*, 115.
- (41) Klimov, V. I. *Appl. Phys. Lett.* **2006**, *89*, 123118/1.
- (42) Nair, G.; Bawendi, M. G. *Phys. Rev. Lett.* **2007**, *76*, 081304.
- (43) Ben-Lulu, M.; Mocatta, D.; Bonn, M.; Banin, U.; Ruhman, S. *Nano Lett.* **2008**, *8*, 1207.
- (44) Shabaev, A.; Efros, A. L.; Nozik, A. J. *Nano Lett.* **2006**, *6*, 2856.
- (45) Rupasov, V. I.; Klimov, V. I. *Phys. Rev. B* **2007**, *76*, 125321/1.
- (46) Schaller, R. D.; Agranovich, V. M.; Klimov, V. I. *Nat. Phys.* **2005**, *1*, 189.
- (47) Prezhdo, O. V. *Chem. Phys. Lett.* **2008**, *460*, 1.
- (48) Franceschetti, A.; An, J. M.; Zunger, A. *Nano Lett.* **2006**, *6*, 2191.
- (49) Allan, G.; Delerue, C. *Phys. Rev. B* **2008**, *77*, 125340.
- (50) Klimov, V. I. *Annu. Rev. Phys. Chem.* **2007**, *58*, 635.
- (51) Nozik, A. J. *Annu. Rev. Phys. Chem.* **2001**, *52*, 193.
- (52) Scholes, G. D. *Annu. Rev. Phys. Chem.* **2003**, *54*, 57.
- (53) Marcus, R. A. *J. Chem. Phys.* **1965**, *43*, 679.
- (54) Newton, M. D. *Chem. Rev.* **1991**, *91*, 767.
- (55) Yu, W. W.; Peng, X. *Angew. Chem., Int. Ed.* **2002**, *41*, 2368.
- (56) Brus, L. *J. Chem. Phys.* **1983**, *79*, 5566.
- (57) Brus, L. E. *J. Chem. Phys.* **1984**, *80*, 4403.
- (58) Klimov, V. I.; Schwarz, C. J.; McBranch, D. W.; Leatherdale, C. A.; Bawendi, M. G. *Phys. Rev. B* **1999**, *60*, R2177.
- (59) Klimov, V. I.; McBranch, D. W.; Leatherdale, C. A.; Bawendi, M. G. *Phys. Rev. B* **1999**, *60*, 13740.

- (60) Klimov, V. I.; Mikhailovsky, A. A.; McBranch, D. W.; Leatherdale, C. A.; Bawendi, M. G. *Science* **2000**, *287*, 1011.
- (61) Klimov, V. I. *J. Phys. Chem. B* **2000**, *104*, 6112.
- (62) Guyot-Sionnest, P. *Struct. Bonding (Berlin, Germany)* **2005**, *118*, 59.
- (63) Beaumont, P. C.; Johnson, D. G.; Parsons, B. J. *J. Photochem. Photobiol. A* **1997**, *107*, 175.
- (64) Guyot-Sionnest, P.; Hines, M. A. *Appl. Phys. Lett.* **1998**, *72*, 686.
- (65) Reynolds, G. A.; Drexhage, K. H. *Opt. Commun.* **1975**, *13*, 222.
- (66) Karstens, T.; Kobs, K. *J. Phys. Chem.* **1980**, *84*, 1871.
- (67) Pons, T.; Medintz, I. L.; Wang, X.; English, D. S.; Mattoussi, H. *J. Am. Chem. Soc.* **2006**, *128*, 15324.
- (68) Tachiya, M. *J. Chem. Phys.* **1982**, *76*, 340.
- (69) Rodgers, M. A. J.; Dasilvaewheeler, M. F. *Chem. Phys. Lett.* **1978**, *53*, 165.
- (70) Marcus, R. A.; Sutin, N. *Biochem. Biophys. Acta* **1985**, *811*, 265.
- (71) Fischer, A. B.; Bronsteinbonte, I. *J. Photochem.* **1985**, *30*, 475.
- (72) Hale, J. M. The Rates of Reactions Involving Only Electron Transfer at Metal Electrodes. In *Reactions of Molecules at Electrodes*; Hush, N. S., Ed.; Wiley-Interscience: New York, 1971; p 229.
- (73) Tavernier, H. L.; Kalashnikov, M. M.; Fayer, M. D. *J. Chem. Phys.* **2000**, *113*, 10191.
- (74) Markel, F.; Ferris, N. S.; Could, I. R.; Myers, A. B. *J. Am. Chem. Soc.* **1992**, *114*, 6208.
- (75) Zimmt, M. B.; Waldeck, D. H. *J. Phys. Chem. A* **2003**, *107*, 3580.
- (76) Du, H.; Fuh, R. C. A.; Li, J. Z.; Corkan, L. A.; Lindsey, J. S. *Photochem. Photobiol.* **1998**, *68*, 141.
- (77) Yu, W. W.; Qu, L.; Guo, W.; Peng, X. *Chem. Mater.* **2003**, *15*, 2854.

JP909972B